A unified scheme for rotation modulation and self-calibration of dual-axis rotating SINS

OPEN ACCESS
IOP Publishing
Measurement Science and Technology
Meas. Sci. Technol. **32** (2021) 115113 (11pp)
https://doi.org/10.1088/1361-6501/ac12ff

A unified scheme for rotation modulation and self-calibration of dual-axis rotating SINS

Huiying Fan, Yuanping Xie, Zichao Wang, Lin Wang, Hui Luo and Xudong Yu*

College of Advanced Interdisciplinary Studies, National University of Defense Technology, Changsha, Hunan 410073, People's Republic of China

E-mail: wind0909@163.com

Received 8 May 2021, revised 7 July 2021
Accepted for publication 9 July 2021
Published 23 July 2021

Abstract

Rotation modulation and self-calibration are the key techniques for error compensation of the strapdown inertial navigation system, which are generally implemented separately. The 16-sequence scheme is widely used for rotation modulation, while the 18-sequence scheme is used for self-calibration. To reduce the complexity of the practical operations, this paper proposes the combination of the rotation modulation scheme and the calibration path and six corresponding design principles of the scheme with both rotation modulation and self-calibration functions. A 48-sequence rotation scheme is designed, which unifies the scheme for self-calibration and rotation modulation. The simulation and experiment results prove that, compared with the 16-sequence rotation modulation scheme, the proposed 48-sequence scheme can reduce the mathematical platform misalignment angle errors and the sawtooth type velocity errors caused by the misalignments of the inertial measurement unit. Besides, its accuracy of self-calibration is better than that of the 18-sequence self-calibration scheme. The velocity errors and position errors can be reduced by about 0.1 m s^{-1} and 0.2 nm in 3 d.

Keywords: rotating SINS, rotation modulation, self-calibration, scheme design principles

(Some figures may appear in color only in the online journal)

1. Introduction

At present, the rotation modulation technique is widely used in high-precision strapdown inertial navigation system (SINS) to eliminate the influence of inertial measurement unit (IMU) errors on the navigation system [1–4]. A reasonable rotation modulation scheme should not only avoid introducing the accumulated navigation errors caused by rotation movements, but also minimize navigation errors caused by drifts, scale-factor errors and misalignments of IMU as much as possible. Compared with the single-axis rotation modulation scheme, the dual-axis rotation scheme modulates the IMU errors on all three axes, and inhibits the accumulation of system errors along with time [5–7]. The shortcomings of error accumulation in the traditional electrostatic gyroscope eight-sequence scheme were analyzed in [8], and a reasonable 16-sequence scheme was designed, which solved the problems of the scale-factor asymmetry, incomplete error elimination and accumulation of calculation errors in the eight-sequence scheme. An improved 16-sequence modulation scheme was proposed in [9]. It can not only modulate the constant drifts, scale-factor errors and misalignments, but also effectively reduce the amplitudes of velocity errors and position errors caused by gyro

* Author to whom any correspondence should be addressed.

misalignments and significantly improve the position accuracy. The 64-sequence scheme proposed in [7] was divided into four short periods, and its effects on modulating the mathematical platform misalignment angle errors caused by the symmetry scale-factor errors is better than those of the 16-sequence scheme. At present, in addition to the widely used 16-sequence scheme proposed in [8], other schemes are not common in practice.

Calibration of inertial sensors is another important technique for error compensation of SINS. By calculating the SINS navigation errors, the precise mathematical relationship between the input and output of IMU is established in the systematic calibration method, and the on-site calibration and self-calibration of SINS are realized [10–15]. The systematic calibration method is better than traditional discrete calibration method as it requires no high-precision turntables and other test equipment, nor does it need to record the output of gyros or accelerometers [16]. Two sets of calibration rotation schemes were designed in [17], which calculated the horizontal and vertical components of the specific force before and after rotation, and estimated the various calibration parameters through the fitting method. A conclusion was drew in [18] that the gyro error parameters are related to the rotation paths and the accelerometer error parameters are only related to the final position. Based on this, a calibration rotation scheme was designed to realize the separation and decoupling between the gyro and accelerometer error parameters. A calibration scheme with 18 sequences designed in [19] is widely used now, which can meet the calibration accuracy requirements of navigation-level SINS within 20 min.

In summary, different rotation schemes are used for error modulation and self-calibration respectively in the existing rotating SINS. When the system needs to be recalibrated, the rotation scheme has to be changed and the turntable has to be restarted. Considering that the design principles of the two kinds of schemes are not contradictory, a 48-sequence rotation scheme for both error modulation and self-calibration is designed in this paper to reduce the complexity of practical operations. The rotation system completes the conversion between error modulation and self-calibration only with the 48-sequence scheme. When the unified 48-sequence scheme is adopted, the switching processes for the rotation scheme between the self-calibration state and the rotation modulation state can be omitted. The unified rotation scheme enables the system to perform rapid emergency re-calibration in response to sudden changes in the environmental conditions.

In the remainder of this paper, the design principles of the unified rotation scheme are put forward first according to the error propagation equations, and then a reasonable 48-sequence rotation scheme is designed. Second, the error propagation characteristics and the observability of the system are analyzed and it is proved that the proposed scheme can realize both the rotation modulation and self-calibration. Finally, the modulation and self-calibration performance of the 48-sequence scheme is compared with that of the 16-sequence modulation scheme and the 18-sequence self-calibration scheme in simulations and experiments, and the conclusions are summarized in the last section.

Table 1. Symbol meanings.

Symbol	Meaning	Symbol	Meaning
n	Navigation frame	p	IMU frame
i	Inertial frame	e	Earth frame
b	Body frame	$\delta\boldsymbol{g}$	Gravity error
$\boldsymbol{\omega}$	Angular rate	$\delta\boldsymbol{\omega}$	Angular rate error
$\boldsymbol{f}$	Specific force	$\delta\boldsymbol{f}$	Specific force error
$\boldsymbol{v}$	Velocity	$\delta\boldsymbol{v}$	Velocity error
$\boldsymbol{C}_p^n$	Transformation matrix from p to n		
$\boldsymbol{\phi}$	Mathematical platform misalignment angle		

2. Design principles of the unified scheme

2.1. Error propagation equations of the rotating SINS

The phi-angle error equations of SINS are adopted to express the error propagation characteristics during the rotation modulation process as follows [20]:

$$\begin{cases} \dot{\boldsymbol{\phi}} = -\boldsymbol{\omega}_{in}^n \times \boldsymbol{\phi} + \delta\boldsymbol{\omega}_{in}^n - \boldsymbol{C}_p^n \delta\boldsymbol{\omega}_{ip}^p \\ \delta\dot{\boldsymbol{v}} = \boldsymbol{f}^n \times \boldsymbol{\phi} + \boldsymbol{C}_p^n \delta\boldsymbol{f}_{ip}^p - (2\boldsymbol{\omega}_{ie}^n + \boldsymbol{\omega}_{en}^n) \times \delta\boldsymbol{v} \\ \qquad -(2\delta\boldsymbol{\omega}_{ie}^n + \delta\boldsymbol{\omega}_{en}^n) \times \boldsymbol{v} + \delta\boldsymbol{g} \end{cases}. \tag{1}$$

The meanings of each symbol in equation (1) are shown in table 1. The purpose of rotation modulation is to make the integrals of the mathematical platform error terms, $\boldsymbol{C}_p^n \delta\boldsymbol{\omega}_{ip}^p$ and $\boldsymbol{C}_p^n \delta\boldsymbol{f}_{ip}^p$, zero in a rotation cycle by periodically changing the value of $\boldsymbol{C}_p^n$, and the impacts of the inertial sensors' accumulated errors on the navigation results are eliminated.

The model of gyro and accelerometer input and output errors is:

$$\begin{cases} \delta\boldsymbol{\omega}_{ip}^p = (\Delta\boldsymbol{S}_g + \Delta\boldsymbol{M}_g)\boldsymbol{\omega}_{ip}^p + \varepsilon \\ \delta\boldsymbol{f}_{ip}^p = (\Delta\boldsymbol{S}_a + \Delta\boldsymbol{M}_a)\boldsymbol{f}_{ip}^p + \nabla \end{cases}, \tag{2}$$

where $\boldsymbol{\omega}_{ip}^p$, ε, ΔS_g and ΔM_g represent the gyro input, drift, scale-factor error and misalignment respectively, and $\boldsymbol{f}_{ip}^p$, ∇, ΔS_a and ΔM_a are the accelerometer input, drift, scale-factor error and misalignment respectively.

Ignoring the translational movement between the body frame and the navigation frame, the navigation frame n, the body frame b and the IMU frame p are coincident at the initial moment, that is $\boldsymbol{C}_p^n = \boldsymbol{C}_b^n = \boldsymbol{C}_p^b = \mathbf{I}$, and $\mathbf{I}$ is the unit matrix. There is always $\boldsymbol{\omega}_{en} = 0$ and $\boldsymbol{\omega}_{nb} = 0$ during the rotation movements. The mathematical platform misalignment angle error caused by gyro errors in a rotation cycle T is:

$$\int_0^T \boldsymbol{C}_p^n \delta\boldsymbol{\omega}_{ip}^p \mathrm{d}t = \int_0^T \boldsymbol{C}_p^n (\Delta\boldsymbol{S}_g + \Delta\boldsymbol{M}_g)\boldsymbol{\omega}_{ip}^p \mathrm{d}t + \int_0^T \boldsymbol{C}_p^n \varepsilon \mathrm{d}t. \tag{3}$$

The gyro error matrix is expressed by $\boldsymbol{E}$ as:

$$\boldsymbol{E} = \Delta\boldsymbol{S}_g + \Delta\boldsymbol{M}_g = \begin{pmatrix} E_{11} & E_{12} & E_{13} \\ E_{21} & E_{22} & E_{23} \\ E_{31} & E_{32} & E_{33} \end{pmatrix}, \tag{4}$$

where E_{11}, E_{22} and E_{33} represent the gyro scale-factor errors, and the other elements in the matrix represent the misalignment errors.

Considering only the coupling between the IMU rotation movements and the errors of inertial sensors, and ignoring the earth's rotation, equation (3) can be transformed into:

$$\int_0^T \boldsymbol{C}_p^n \delta\boldsymbol{\omega}_{ip}^p \mathrm{d}t = \int_0^T \boldsymbol{C}_p^n \boldsymbol{E}\boldsymbol{\omega}_{np}^p \mathrm{d}t + \int_0^T \boldsymbol{C}_p^n \varepsilon \mathrm{d}t. \tag{5}$$

2.2. Design principles of the unified scheme

To design a unified scheme that can simultaneously realize dual-axis rotation modulation and self-calibration, the following principles need to be followed:

2.2.1. The principle of centrosymmetric track. The drifts of the three gyros can be regarded as a constant vector $\vec{\varepsilon} = (\ \varepsilon_x \quad \varepsilon_y \quad \varepsilon_z\ )^{\mathrm{T}}$ in the IMU frame. When the error modulation scheme is executed, $\vec{\varepsilon}$ rotates regularly in the navigation frame. The track of $\vec{\varepsilon}$ should be symmetrical about its geometric center to eliminate the accumulated errors of the inertial sensors' drifts. In addition, the rotation rates, rotation accelerations, dwell positions and dwell duration in symmetrical positions should all be completely symmetrical to ensure that the integral of $\vec{\varepsilon}$ in the navigation frame, $\int_0^T \boldsymbol{C}_p^n \varepsilon \mathrm{d}t$, is equal to 0.

2.2.2. The principle of opposite rotation directions on the same track. As is shown in figure 1, when the movement trajectory of $\vec{\varepsilon}$ is from position 'a' to position 'b', the relationship between the rotation angle and the rotation time is $\theta = \omega_0 t$, where ω_0 is the magnitude of rotation angular rate, and the total rotation time is T_0. The mathematical platform misalignment angle error caused by the scale-factor errors and misalignments of the gyros is:

$$\int_0^{T_0} \boldsymbol{C}_p^n \boldsymbol{E}\boldsymbol{\omega}_{np}^p \mathrm{d}t = \frac{1}{\boldsymbol{\omega}_0} \int_{\theta_1}^{\theta_2} \boldsymbol{C}_p^n \boldsymbol{E}\boldsymbol{\omega}_{np}^p \mathrm{d}\theta. \tag{6}$$

When the movement trajectory is from 'b' to 'a', the magnitude of rotation angular rate is the same as above, but the direction is opposite. The relationship between the rotation angle and the rotation time is $\theta = -\omega_0 t$. The misalignment angle error caused by the scale-factor errors and misalignments is:

$$\begin{aligned} \int_0^{T_0} \boldsymbol{C}_p^n \boldsymbol{E}\boldsymbol{\omega}_{np}^p \mathrm{d}t &= -\frac{1}{\boldsymbol{\omega}_0} \int_{\theta_2}^{\theta_1} \boldsymbol{C}_p^n \boldsymbol{E}(-\boldsymbol{\omega}_{np}^p) \mathrm{d}\theta \\ &= -\frac{1}{\boldsymbol{\omega}_0} \int_{\theta_1}^{\theta_2} \boldsymbol{C}_p^n \boldsymbol{E}\boldsymbol{\omega}_{np}^p \mathrm{d}\theta. \end{aligned} \tag{7}$$

Actually, there are angular accelerations between position 'a' and 'b' (positive and negative) to reach ω_0 and to stop rotation. The angular accelerations should be equal in clockwise and counter-clockwise rotations as much as possible to keep the integral equation (6) equal to integral equation (7).

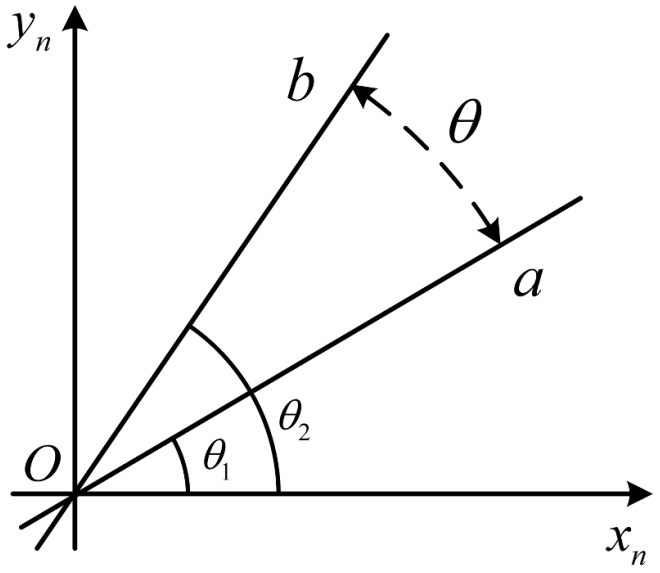

Figure 1. Movement trajectory of the drift vector.

Therefore, an inverse path should be added on the same track when designing a unified scheme to offset the accumulated errors in the forward path caused by the gyro scale-factor errors and the misalignments. The rotating directions of the two paths on the same track should be opposite so as to modulate the scale-factor errors and misalignments.

2.2.3. The principle of opposite rotation directions around the same axis. In order to enhance the effects of the scheme on modulating the inertial sensors' errors, the mean value of the mathematical platform misalignment angle errors in a rotation cycle should be reduced as much as possible. When the IMU rotates in reverse around a rotation axis, the period during which the misalignment angle errors caused by the IMU scale-factor errors, asymmetry scale-factor errors and misalignments are modulated to 0 is shortened. Therefore, the directions of the two sequences rotating around the same axis should be opposite in small periods of $T/2$ or $T/4$ to shorten the modulation cycle of inertial sensors' errors.

2.2.4. The principle of alternate rotating and dwelling. The IMU should keep stationary for a while after rotating a certain angle. It helps to reduce the additional control errors caused by the continuous operations of the rotating mechanism. At the same time the drift errors of the gyros and accelerometers are easily excited during the dwell period.

2.2.5. The principle of three axis rotations. When the IMU rotates 180° around the x, y, or z axis respectively in the IMU frame, the misalignment angle errors caused by the gyro scale-factor errors and misalignments are:

$$\Delta\boldsymbol{\phi}_x = \begin{pmatrix} \pi E_{11} \\ -2E_{31} \\ 2E_{21} \end{pmatrix}, \Delta\boldsymbol{\phi}_y = \begin{pmatrix} 2E_{32} \\ \pi E_{22} \\ -2E_{12} \end{pmatrix}, \Delta\boldsymbol{\phi}_z = \begin{pmatrix} -2E_{23} \\ 2E_{13} \\ \pi E_{33} \end{pmatrix}. \quad (8)$$

It can be seen that only one scale-factor error and two misalignments can be excited for every 180° rotation around an IMU sensitive axis. All the scale-factor errors and misalignments of gyros can be excited only if the IMU rotates around all the three sensitive axes.

2.2.6. The principle of three axes up-and-down flips. When the three sensitive axes of the accelerometers point to the sky and the ground in turn (parallel to gravity), the drifts, scale-factor errors and misalignments of the accelerometers can be excited. Therefore, there should be sequences that rotate 180° in total around the horizontal axis to realize the up-and-down flips of the sensitive axes, and there should be sequences that rotate 90° around the horizontal axis to exchange the flip axes.

2.3. Design of the rotation scheme

According to the principles proposed above, a unified 48-sequence scheme is designed. The rotation process is shown in figure 2, where the U and E are the upward axis and eastward axis in the navigation frame. $A \sim D$ and $A' \sim D'$ are eight dwell positions. The dotted lines represent the rotation movement tracks of the drift vector $\vec{\varepsilon}$, and $1 \sim 48$ represent 48 rotation sequences. The detailed rotation scheme is shown in table 2.

3. Analysis of errors and observability

3.1. Error analysis

In order to prove that the 48-sequence rotation scheme can realize error modulation and observe its modulation effects, this section will take the gyro errors as an example to analyze its propagation characteristics.

3.1.1. Analysis of mathematical platform misalignment angle errors. According to equation (5), the mathematical platform misalignment angle errors caused by $\boldsymbol{E}$ of the 48-sequence scheme in a rotation cycle can be calculated as follows:

$$\begin{aligned}\int_0^{T/2} \boldsymbol{C}_p^n \boldsymbol{E} \omega_{np}^p \mathrm{d}t &= \sum_{i=1}^{24} \left(\int_{(i-1)T/48}^{iT/48} \boldsymbol{C}_p^n(t) \boldsymbol{E} \begin{pmatrix} \omega_x \\ \omega_y \\ \omega_z \end{pmatrix} \mathrm{d}t \right) \\ &= \begin{pmatrix} \frac{\pi}{2}E_{11} \\ E_{21}-E_{31} \\ E_{21}+E_{31} \end{pmatrix} + \begin{pmatrix} -2E_{23} \\ -\pi E_{33} \\ 2E_{13} \end{pmatrix} + \begin{pmatrix} -\frac{\pi}{2}E_{11} \\ -E_{21}-E_{31} \\ -E_{21}+E_{31} \end{pmatrix} + \begin{pmatrix} -2E_{23} \\ \pi E_{22} \\ -2E_{12} \end{pmatrix} \\ &\quad + \begin{pmatrix} \frac{\pi}{2}E_{11} \\ -E_{21}+E_{31} \\ -E_{21}-E_{31} \end{pmatrix} + \begin{pmatrix} -2E_{23} \\ \pi E_{33} \\ -2E_{13} \end{pmatrix} + \begin{pmatrix} -\frac{\pi}{2}E_{11} \\ E_{21}+E_{31} \\ E_{21}-E_{31} \end{pmatrix} + \begin{pmatrix} -2E_{23} \\ -\pi E_{22} \\ 2E_{12} \end{pmatrix} + \cdots = \begin{pmatrix} 0 \\ 0 \\ 0 \end{pmatrix} \end{aligned}$$

$$\begin{aligned}\int_{T/2}^{T} \boldsymbol{C}_p^n \boldsymbol{E} \omega_{np}^p \mathrm{d}t &= \sum_{i=25}^{48} \left(\int_{(i-1)T/48}^{iT/48} \boldsymbol{C}_p^n(t) \boldsymbol{E} \begin{pmatrix} \omega_x \\ \omega_y \\ \omega_z \end{pmatrix} \mathrm{d}t \right) \\ &= \begin{pmatrix} 2E_{32} \\ -\pi E_{22} \\ -2E_{12} \end{pmatrix} + \begin{pmatrix} \frac{\pi}{2}E_{11} \\ -E_{21}-E_{31} \\ -E_{21}+E_{31} \end{pmatrix} + \begin{pmatrix} 2E_{23} \\ \pi E_{33} \\ 2E_{13} \end{pmatrix} + \begin{pmatrix} -\frac{\pi}{2}E_{11} \\ E_{21}-E_{31} \\ E_{21}+E_{31} \end{pmatrix} \\ &\quad + \begin{pmatrix} 2E_{32} \\ \pi E_{22} \\ 2E_{12} \end{pmatrix} + \begin{pmatrix} \frac{\pi}{2}E_{11} \\ E_{21}+E_{31} \\ E_{21}-E_{31} \end{pmatrix} + \begin{pmatrix} 2E_{23} \\ -\pi E_{33} \\ -2E_{13} \end{pmatrix} + \begin{pmatrix} -\frac{\pi}{2}E_{11} \\ -E_{21}+E_{31} \\ -E_{21}-E_{31} \end{pmatrix} + \cdots = \begin{pmatrix} 0 \\ 0 \\ 0 \end{pmatrix}. \quad (9)\end{aligned}$$

Therefore, the misalignment angle error in a rotation cycle is $\int_0^T \boldsymbol{C}_p^n \boldsymbol{E} \omega_{np}^p \mathrm{d}t = 0$. It indicates that the mathematical platform misalignment angle error caused by gyro error $\boldsymbol{E}$ is modulated to zero within $T/2$ in this scheme, and there is no accumulated error in a rotation cycle. The purpose of error modulation can be achieved. In addition, according to the proposed principle of centrosymmetric track, there is $\int_0^T \boldsymbol{C}_p^n \boldsymbol{\varepsilon} \mathrm{d}t = 0$, which should not be repeated here.

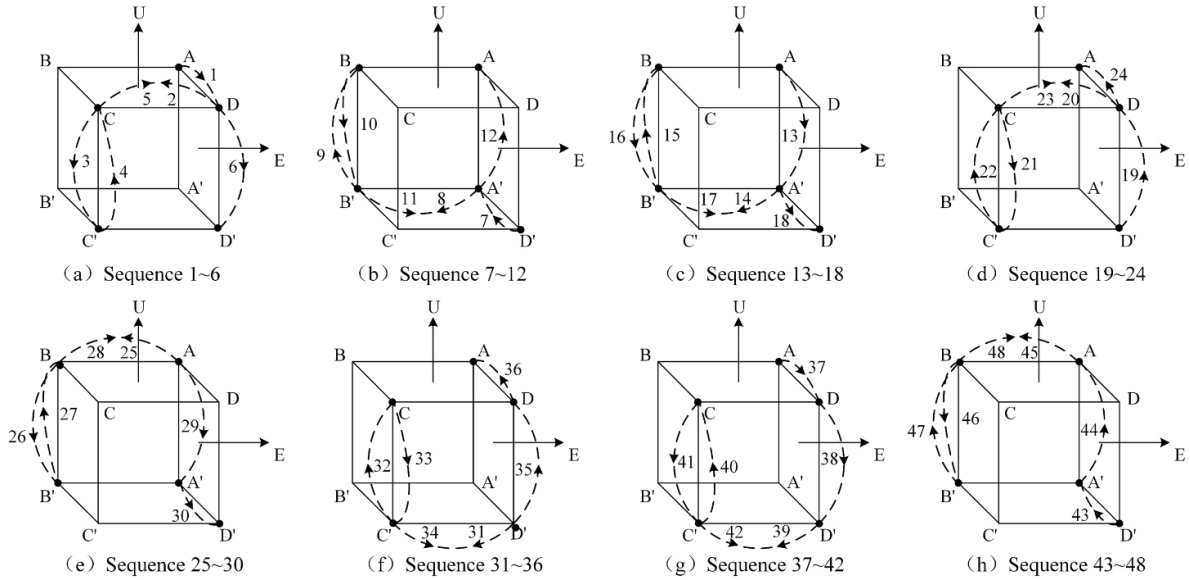

Figure 2. The unified 48-sequence rotation scheme.

Table 2. The detailed rotation scheme.

Sequence	Rotation path	Rotation angle	
		In navigation frame	In IMU frame
1	$A \to D$	$+90°$E	$+90°$X
2, 3	$D \to C \to C'$	$-180°$N	$+180°$Z
4	$C' \to C$	$-90°$E	$+90°$X
5, 6	$C \to D \to D'$	$+180°$N	$-180°$Y
7	$D' \to A'$	$+90°$E	$+90°$X
8, 9	$A' \to B' \to B$	$+180°$N	$+180°$Z
10	$B \to B'$	$+90°$E	$+90°$X
11, 12	$B' \to A' \to A$	$-180°$N	$-180°$Y
13 $\sim$ 24	Inverse paths of 1 $\sim$ 12 sequences		
25, 26	$A \to B \to B'$	$-180°$N	$-180°$Y
27	$B' \to B$	$+90°$E	$-90°$X
28, 29	$B \to A \to A'$	$+180°$N	$+180°$Z
30	$A' \to D'$	$-90°$E	$-90°$X
31, 32	$D' \to C' \to C$	$+180°$N	$-180°$Y
33	$C \to C'$	$+90°$E	$-90°$X
34, 35	$C' \to D' \to D$	$-180°$N	$+180°$Z
36	$D \to A$	$-90°$E	$-90°$X
37 $\sim$ 48	Inverse paths of 25 $\sim$ 36 sequences		

3.1.2. Analysis of sawtooth type velocity errors. In a short period, ignoring the mathematical platform misalignment angle errors caused by the Earth's rotation and the drifts, according to equation (1), the misalignment angle errors caused by $\boldsymbol{E}$ at the moment will be coupled with gravity, and the mathematical platform acceleration errors are produced as follows:

$$\delta\dot{\boldsymbol{v}}_{\mathrm{E}} = g\int_0^t \Delta\boldsymbol{\phi}_{\mathrm{N}}\mathrm{d}t,\ \delta\dot{\boldsymbol{v}}_{\mathrm{N}} = -g\int_0^t \Delta\boldsymbol{\phi}_{\mathrm{E}}\mathrm{d}t, \tag{10}$$

where $\Delta\boldsymbol{\phi}_{\mathrm{E}}$ and $\Delta\boldsymbol{\phi}_{\mathrm{N}}$ are the equivalent mathematical platform misalignment angle errors in the east and north directions caused by $\boldsymbol{E}$ respectively. Then the mathematical platform velocity errors at the moment t are:

$$\delta\boldsymbol{v}_{\mathrm{E}} = \int_0^t \left(g\int_0^t \Delta\boldsymbol{\phi}_{\mathrm{N}}\mathrm{d}t\right)\mathrm{d}t,\ \delta\boldsymbol{v}_{\mathrm{N}} = \int_0^t \left(-g\int_0^t \Delta\boldsymbol{\phi}_{\mathrm{E}}\mathrm{d}t\right)\mathrm{d}t. \tag{11}$$

The sawtooth type velocity errors caused by the gyro scale-factor errors and misalignments of gyros are calculated in table 3. It shows the accumulated eastward sawtooth type velocity errors in the 16-sequence scheme and the 48-sequence scheme during the dwell period at each position, which stay T_S seconds after each rotation.

Table 3. Eastward sawtooth type velocity errors.

Sequence	16-sequence scheme	Sequence	48-sequence scheme
1	$2E_{13}gT_S$	1	$(E_{21}-E_{31})gT_S$
2	$(4E_{13}+2E_{31})gT_S$	2, 3	$[3E_{21}-3E_{31}-2\pi E_{33}]\,gT_S$
3	$(8E_{13}+4E_{31})gT_S$	4	$[3E_{21}-5E_{31}-3\pi E_{33}]\,gT_S$
4	$(12E_{13}+8E_{31})gT_S$	5, 6	$[3E_{21}-9E_{31}-5\pi E_{33}-2\pi E_{22}]\,gT_S$
5	$(16E_{13}+10E_{31})gT_S$	7	$[2E_{21}-10E_{31}-6\pi E_{33}+3\pi E_{22}]\,gT_S$
6	$(18E_{13}+12E_{31})gT_S$	8, 9	$[-12E_{31}-6\pi E_{33}+5\pi E_{22}]\,gT_S$
7	$(20E_{13}+12E_{31})gT_S$	10	$[-12E_{31}-6\pi E_{33}+6\pi E_{22}]\,gT_S$
8	$(20E_{13}+12E_{31})gT_S$	11, 12	$[-12E_{31}-6\pi E_{33}+6\pi E_{22}]\,gT_S$
9	$(22E_{13}+12E_{31})gT_S$	13, 14	$[-12E_{31}-6\pi E_{33}+8\pi E_{22}]\,gT_S$
10	$(24E_{13}+14E_{31})gT_S$	…	…
11	$(28E_{13}+16E_{31})gT_S$	…	…
12	$(32E_{13}+20E_{31})gT_S$	41, 42	$[3E_{21}-45E_{31}-\pi E_{33}+4\pi E_{22}]\,gT_S$
13	$(36E_{13}+22E_{31})gT_S$	43	$[2E_{21}-46E_{31}+3\pi E_{22}]\,gT_S$
14	$(38E_{13}+24E_{31})gT_S$	44, 45	$[-48E_{31}+\pi E_{22}]\,gT_S$
15	$(40E_{13}+24E_{31})gT_S$	46	$-48E_{31}gT_S$
16	$(40E_{13}+24E_{31})gT_S$	47, 48	$-48E_{31}gT_S$
Mean value	$(5/2E_{13}+3/2E_{31})gT_S$	Mean value	$-E_{31}gT_S$

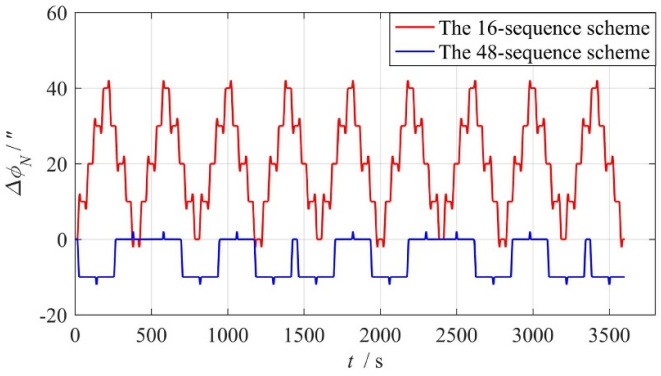

Figure 3. Northward mathematical platform misalignment angle errors.

As shown in table 3, the average eastward sawtooth type velocity error in the 16-sequence scheme is $(5/2E_{13}+3/2E_{31})gT_S$, worse than $-E_{31}gT_S$ in the 48-sequence scheme. Moreover, the maximum value of the sawtooth type velocity errors in the 48-sequence scheme is also smaller than that in the 16-sequence scheme for laser gyros with smaller scale-factor errors. It indicates that the 48-sequence scheme has better effects on modulating the misalignments, and the sawtooth type velocity errors caused by the misalignment errors are smaller.

Figure 3 shows the northward mathematical platform angle errors caused by the gyro misalignments ($5''$) of the 16-sequence scheme and the 48-sequence scheme within one hour. It can be seen that both the mean value and maximum value of the northward mathematical platform angle errors in the 48-sequence scheme are smaller than those in the 16-sequence scheme. It can be inferred that the 48-sequence rotation scheme will reduce the sawtooth type velocity errors caused by the coupling between the mathematical platform misalignment angle errors and gravity.

3.2. Observability analysis

In order to determine the feasibility of this scheme which calibrates the error parameters of inertial sensors, the observability analysis based on piece-wise constant system and degree of observability analysis based on singular value decomposition will be carried out in this section [21–26].

A 30-dimensional Kalman filter calibration equation is established as follows:

$$\dot{X}(t) = A(t)X(t) + W(t), \tag{12}$$

where $X(t)$ represents the state vector, $A(t)$ is the system matrix and $W(t)$ is the excitation noise. The state vector is set as follows:

$$X(t) = \begin{bmatrix} \phi_E & \phi_N & \phi_D & \delta v_E & \delta v_N & \delta v_D \\ \delta L & \delta\lambda & \delta h & \varepsilon_x & \varepsilon_y & \varepsilon_z \\ \nabla_x & \nabla_y & \nabla_z & \Delta S_{gx} & \Delta M_{gyx} & \Delta M_{gzx} \\ \Delta S_{gy} & \Delta M_{gzy} & \Delta S_{gz} & \Delta S_{ax} & \Delta M_{ayx} & \Delta M_{azx} \\ \Delta M_{axy} & \Delta S_{ay} & \Delta M_{azy} & \Delta M_{axz} & \Delta M_{ayz} & \Delta S_{az} \end{bmatrix}^{\mathrm{T}}, \tag{13}$$

where δL, $\delta\lambda$ and δh are the latitude error, longitude error and altitude error respectively.

After the piecewise linearization of the system, observability is analyzed by using the stripped observability matrix (SOM) instead of the total observability matrix. The ranks of SOM at each position in the 18-sequence scheme and the 48-sequence scheme are calculated, and the results are shown in table 4.

It can be seen from table 4 that after four rotation sequences, the rank of the SOM in the 48-sequence scheme reaches 30, which is equal to the dimensionality of the Kalman filter, and

Table 4. Ranks of the stripped observability matrix (SOM).

Position	18-sequence scheme	48-sequence scheme
0	12	12
1	18	17
2	23	23
3	23	29
4	29	30
5	30	30
6	30	30
…	30	30
18	30	30
…	—	30
48	—	30

Table 5. Singular values of parameters.

Parameter	18-sequence scheme	48-sequence scheme
ε_x	40.37	40.33
ε_y	38.94	39.16
ε_z	38.56	39.16
∇_x	34.60	39.16
∇_y	27.60	39.16
∇_z	9.89	9.89
ΔS_{gx}	8.06	8.11
ΔS_{gy}	7.00	7.00
ΔS_{gz}	7.00	7.00
ΔS_{ax}	7.00	7.00
ΔS_{ay}	0.0022	0.0029
ΔS_{az}	0.0009	0.0018
ΔM_{gyx}	7.58	8.05
ΔM_{gzx}	7.05	8.05
ΔM_{gzy}	7.00	7.00
ΔM_{axy}	0.0032	0.0036
ΔM_{axz}	0.0014	0.0022
ΔM_{ayz}	0.0014	0.0018
ΔM_{ayx}	7.00	7.00
ΔM_{azx}	0.0035	0.0044
ΔM_{azy}	0.0019	0.0029

it is proved that the system is completely observable. In addition, the rank of the SOM in the 48-sequence scheme reaches 30 one sequence earlier than that of the 18-sequence scheme SOM, indicating that the 48-sequence scheme can observe all the parameters earlier.

The singular value of the SOM is positively correlated with the degree of observability. The singular values of each error parameter after 48 sequence rotations in the 18-sequence scheme and the 48-sequence scheme are shown in table 5.

Most of the parameters in the 48-sequence scheme have larger singular values than those in the 18-sequence, which indicates that the 48-sequence scheme has higher degree of observability and its calibration results are easier to approach the actual values.

Table 6. Parameters used for simulations.

Parameter		Value
Gyro	Drift	$0.01^\circ\ \mathrm{h}^{-1}$
	Scale-factor error	1 ppm
	Misalignment	$5''$
	Random walk	$0.002^\circ\ /\sqrt{(\mathrm{h})}$
Accelerometer	Drift	10 μg
	Scale-factor error	5 ppm
	Misalignment	$5''$
	Second-order non-linearity error	5 $\mu g/\mathrm{g}^2$

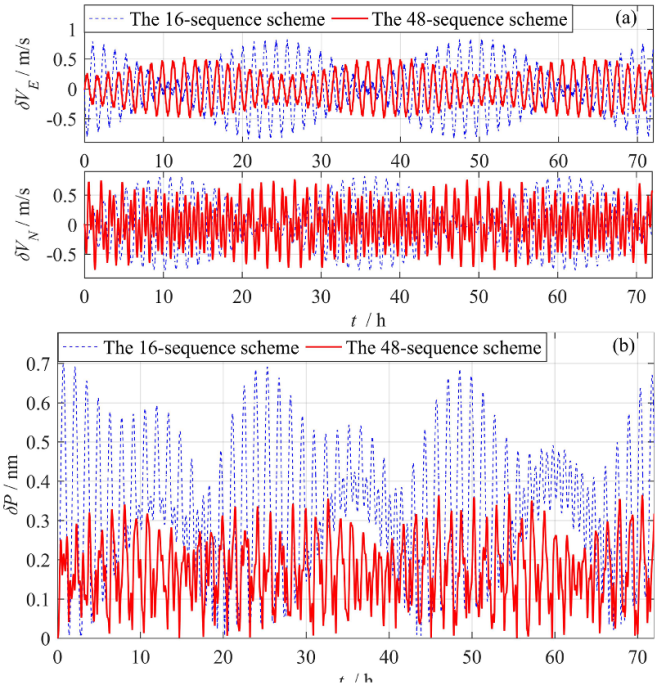

Figure 4. (a) Velocity errors and (b) position errors of the 18-sequence scheme and the 48-sequence scheme.

4. Verification of simulations and experiments

4.1. Simulation verification

4.1.1. Simulation verification of rotation modulation. In order to compare the effects of the 16-sequence scheme and the proposed 48-sequence scheme on modulating the inertial sensors' errors, the navigation simulations are carried out, and the error parameters are set as table 6.

Figure 4(a) respectively shows the eastward and northward velocity errors of the two schemes after three-day rotation modulation simulations, and figure 4(b) shows the navigation position errors of the two schemes. The maximum eastward and northward velocity errors of the 16-sequence scheme are 0.82 and 0.81 m s^{-1}, and the maximum position error is 0.69 nm. The maximum eastward and northward velocity errors of the 48-sequence scheme are 0.53 and 0.76 m s^{-1} respectively, and the maximum position error is 0.36 nm. The

Table 7. Simulation results of self-calibration.

Parameter	Actual value	18-sequence scheme	48-sequence scheme
ε_x (°/h)	0.01	0.0086	0.0098
ε_y (°/h)	0.01	0.0088	0.0101
ε_z (°/h)	0.01	0.0101	0.0099
∇_x μg	50	50.01	50.00
∇_y μg	50	49.99	49.99
∇_z μg	50	49.99	50.00
ΔS_{gx} (ppm)	10	9.44	9.98
ΔS_{gy} (ppm)	20	19.34	20.03
ΔS_{gz} (ppm)	30	30.03	29.94
ΔS_{ax} (ppm)	10	10.06	10.01
ΔS_{ay} (ppm)	20	20.03	20.03
ΔS_{az} (ppm)	30	30.02	30.03
ΔM_{gyx} ($''$)	10	10.12	9.99
ΔM_{gzx} ($''$)	20	20.18	19.99
ΔM_{gzy} ($''$)	30	30.00	30.00
ΔM_{axy} ($''$)	−30	−30.03	−29.99
ΔM_{axz} ($''$)	10	9.83	10.03
ΔM_{ayz} ($''$)	−20	−20.02	−19.98
ΔM_{ayx} ($''$)	10	10.02	9.97
ΔM_{azx} ($''$)	−20	−19.86	−20.02
ΔM_{azy} ($''$)	30	30.04	29.99

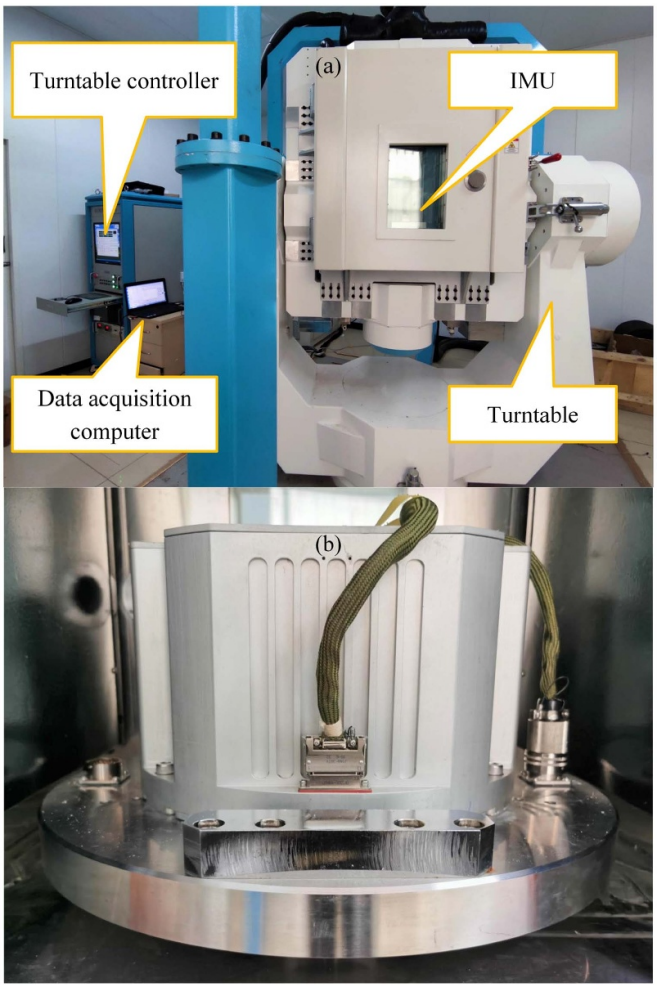

Figure 5. Diagrams of (a) the experimental system and (b) the IMU.

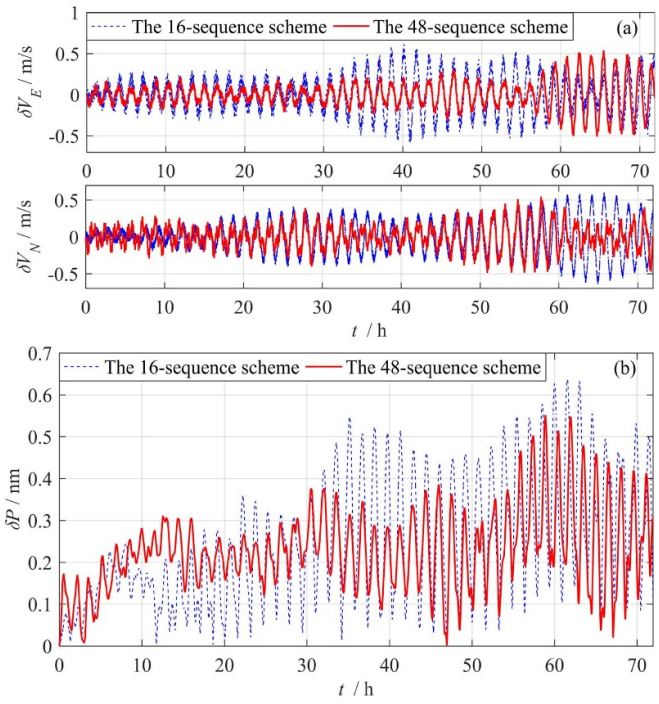

Figure 6. (a) Velocity errors and (b) position errors of experiment 1 and experiment 2.

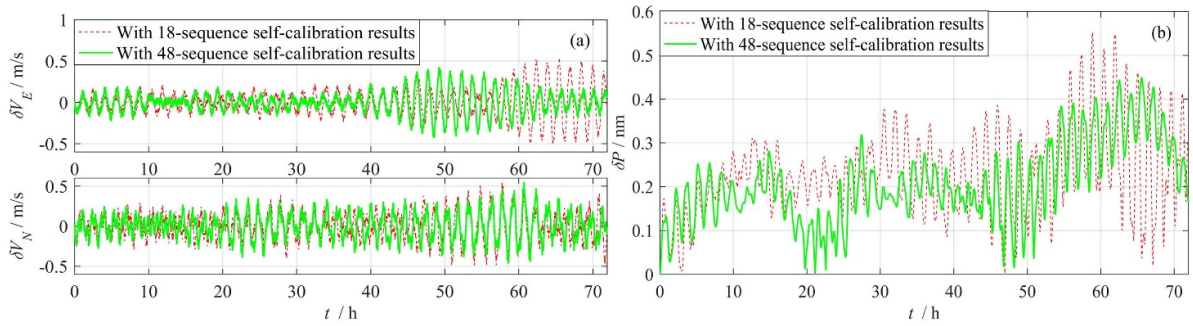

Figure 7. (a) Velocity errors and (b) position errors of experiment 2 and experiment 3.

navigation errors of 48-sequence scheme are obviously smaller than those of the 16-sequence scheme, which indicates that the 48-sequence scheme has better rotation modulation effects.

4.1.2. Simulation verification of self-calibration. In order to compare the effects of the 18-sequence scheme and the 48-sequence scheme on calibrating the inertial sensors' error parameters, the self-calibration simulations are carried out. The results are shown in table 7. It can be seen that the calibration results of the scheme proposed in this paper are closer to the actual values.

4.2. Experiment verification

In order to verify the navigation performance of the unified scheme proposed in this paper, laboratory experiments are carried out, and the experimental system is shown in figure 5(a), which is composed of an IMU, a turntable, a turntable controller and a data acquisition computer. The IMU shown in figure 5(b) consists of three ring laser gyroscopes with bias stability of 0.003° h^{-1} and three quartz accelerometers with bias stability of 10 μg.

Considering that the scale-factor nonlinearity errors and asymmetry errors can be modulated by the proposed scheme, and the scale-factor nonlinearity errors and asymmetry errors of laser gyros in our actual IMU system are small (0.09 ppm), and the vehicle angular rate is small in the practical application environments, the negligible influences of the gyro scale-factor nonlinearity errors and asymmetry errors on the calibration, initial alignment and rotation modulation processes will be ignored in this paper.

The following three groups of experiments are implemented:

(a) Navigation experiments with 16-sequence rotation modulation and 18-sequence self-calibration results;
(b) navigation experiments with 48-sequence rotation modulation and 18-sequence self-calibration results;

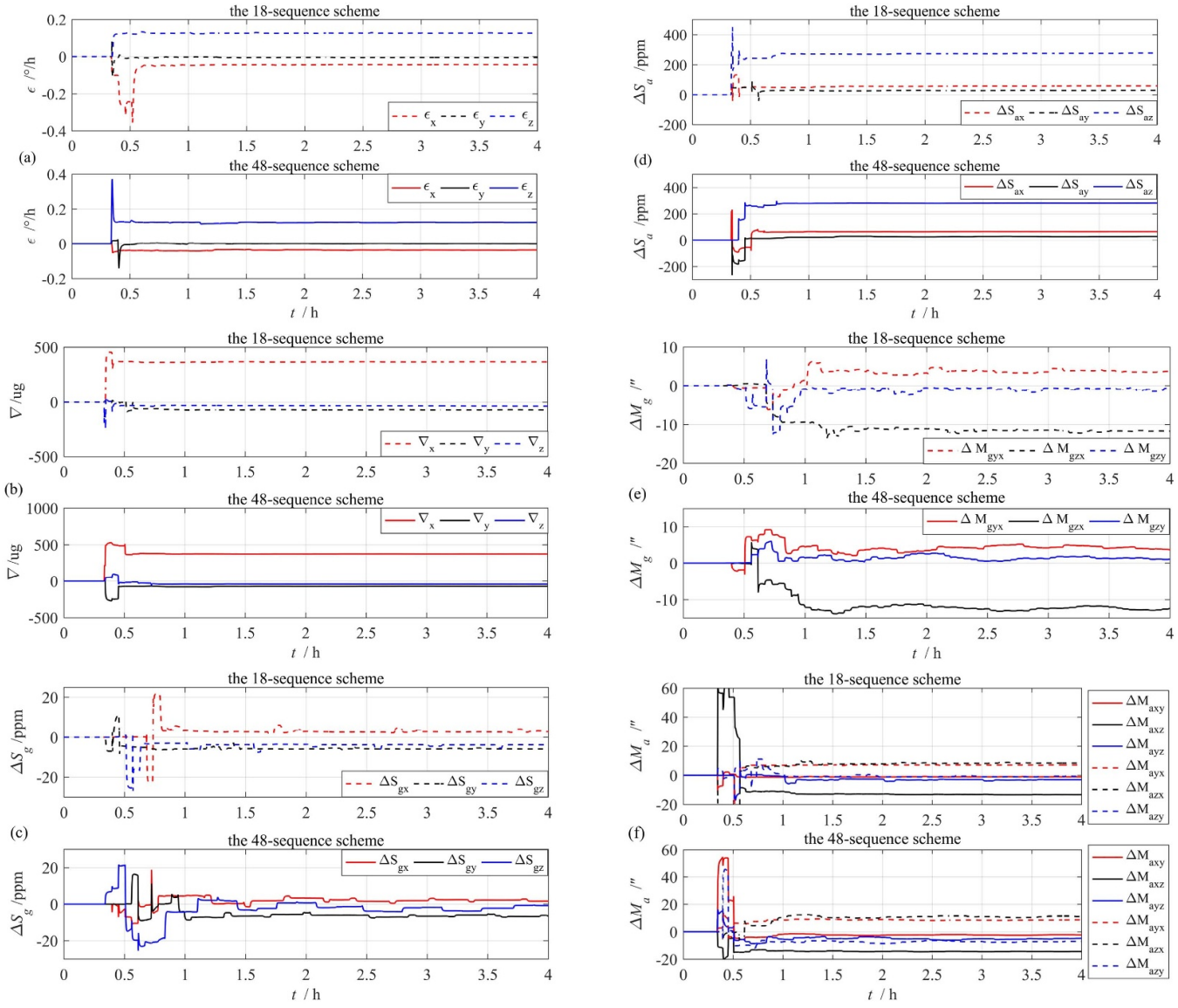

Figure 8. The self-calibration curves of the 18-sequence scheme and the 48-sequence scheme.

(c) navigation experiments with 48-sequence rotation modulation and 48-sequence self-calibration results.

The results of experiment 1 and experiment 2 are shown in figure 6. It can be seen that the proposed 48-sequence scheme reduce the velocity and position errors by about 0.1 m s^{-1} and 0.1 nm, and it has a better error modulation performance than the 16-sequence scheme with the same self-calibration results. The results of experiment 2 and experiment 3 are shown in figure 7. When the 48-sequence scheme is used for both rotation modulation and self-calibration processes, the position errors are reduced by 0.1 nm again, which indicates that the proposed 48-sequence scheme has a better self-calibration performance than the 18-sequence scheme, and the self-calibration curves are shown in figure 8.

5. Conclusion

This paper focuses on a unified scheme for both rotation modulation and self-calibration of dual-axis rotating SINS. The design principles of the unified scheme are put forward according to the error propagation equations of SINS and a detailed 48-sequence rotation scheme is designed. Then the errors and the observability are analyzed. It is indicated that the proposed scheme can compensate all the drifts, scale-factor errors and misalignments of the inertial sensors and causes no error accumulation. The mathematical platform misalignment angle errors and the sawtooth type velocity errors are smaller than those of the 16-sequence rotation modulation scheme, and the observability of the system is better than that of the 18-sequence self-calibration scheme. The simulation and experiment results show that the modulation performance of the proposed scheme is better and the self-calibration results are

closer to the actual values, which causes a velocity error reduction of 0.1 m s^{-1} and a position error reduction of 0.2 nm in 3 d.

Data availability statement

All data that support the findings of this study are included within the article (and any supplementary files).

Acknowledgments

This work is supported by the National Natural Science Foundation of China (Grant No. 62003360).

ORCID iDs

Huiying Fan https://orcid.org/0000-0002-8372-8886
Zichao Wang https://orcid.org/0000-0001-8346-7033
Xudong Yu https://orcid.org/0000-0002-3082-0830

References

[1] Yuan B and Rao G 2006 On the theory of optical gyro rotating inertial navigation system *J. Natl Univ. Def. Technol.* **28** 76–80
[2] Yu X, Wang Y, Zhang P, Tang J and Long X 2008 Influence of single-axial rotation on INS error characteristics *J. Chin. Inertial Technol.* **16** 643–8
[3] Yang Y and Miao L 2004 Fiber-optic strapdown inertial system with sensing cluster continuous rotation *IEEE Trans. Aerosp. Electron. Syst.* **40** 1173–8
[4] Levinson E and Majure R 1987 Accuracy enhancement techniques applied to the marine ring laser inertial navigator (MARLIN) *Navigation* **34** 64–86
[5] Lei H, Wang X and Liu F 2016 Analysis on error characteristics and key technology of airborne double-axis rotation-modulating RLG INS *Navig. Position. Timing* **3** 13–8
[6] Weng H, Lu Q, Huang K, Zhang Y and Yang G 2009 Rotation scheme design for rotary optical gyro SINS *J. Chin. Inertial Technol.* **17** 8–14
[7] Wang Z, Yin H and Wang D 2013 Rotating scheme designing for two-axis rotating laser gyro inertial navigation system *Ship Sci. Technol.* **35** 114–20
[8] Yuan B, Liao D and Han S 2012 Error compensation of an optical gyro INS by multi-axis rotation *Meas. Sci. Technol.* **23** 025102
[9] Ji Z, Liu C, Cai S, Xu H and Zhou Z 2013 Improved sixteen-sequence rotation scheme for dual-axis SINS *J. Chin. Inertial Technol.* **21** 46–50
[10] Lu Z and Wang X 2010 Error analysis and calibration of systematic dual-axis rotation-modulating SINS *J. Chin. Inertial Technol.* **18** 135–41
[11] Quan Z, Shi Z and Wang Y 2012 Online calibration technology for strapdown inertial navigation system *Modern Electron. Tech.* **35** 128–31
[12] Yang X and Huang Y 2008 Systematic calibration method for laser gyro SINS *J. Chin. Inertial Technol.* **16** 1–7
[13] Lin Y and Deng Z 2001 Systematic calibration for inertial instruments errors in laser gyro strapdown inertial navigation system *J. Harbin Inst. Technol.* **33** 112–6
[14] Zhou Q, Qin Y, Yan G and Yang P 2008 Precision calibration techniques research for laser strap-down inertial measurement unit *Meas. Control Technol.* **27** 95–8
[15] Grewal M S, Henderson V D and Miyasako R S 1991 Application of Kalman filtering to the calibration and alignment of inertial navigation systems *IEEE Trans. Autom. Control.* **36** 4–13
[16] Pittman D N and Roberts C E 1992 Determining inertial errors from navigation-in-place data *IEEE Position Location and Navigation Symp.* pp 60–7
[17] Savage P G 2007 *Strapdown Analytics* 2nd edn (Maple Plain: Strapdown Associates Inc.)
[18] Mark J, Tazartes D and Hilby T 1986 Fast orthogonal calibration of a ring laser strapdown system *Symp. Gyro Technology* pp 13.0–13.21
[19] Camberlein L and Mazzanti F 1985 Calibration technique for laser gyro strapdown inertial navigation systems *Symp. Gyro Technology* (*Stuttgart, Germany*)
[20] Titterton D H and Weston J L 2004 *Strapdown Inertial Navigation Technology* 2nd edn (Reston, VA: American Institute of Aeronautics and Astronautics/ Institution of Electrical Engineers) pp 14–29
[21] Goshen-Meskin D and Bar-Itzhack I Y 1992 Observability analysis of piece-wise constant systems-part I: theory *IEEE Trans. Aerosp. Electron. Syst.* **28** 1056–67
[22] Goshen-Meskin D and Bar-Itzhack I Y 1992 Observability analysis of piece-wise constant systems-part II: application to inertial navigation in-flight alignment *IEEE Trans. Aerosp. Electron. Syst.* **28** 1068–75
[23] Pecht E and Mintchev M P 2007 Observability analysis for INS alignment in horizontal drilling *IEEE Trans. Instrum. Meas.* **56** 1935–45
[24] Pecht E and Mintchev M P 2007 Modeling of observability during in-drilling alignment for horizontal directional drilling *IEEE Trans. Instrum. Meas.* **56** 1946–54
[25] Cao Y, Cai H, Zhang S and Li A 2012 A new continuous self-calibration scheme for a gimbaled inertial measurement unit *Meas. Sci. Technol.* **23** 1–9
[26] Cheng X, Wan D and Zhong X 1997 Study on observability and its degree of strapdown inertial navigation system *J. Southeast Univ.* **27** 6–11